In: TMS 2026 155th Annual Meeting & Exhibition Supplemental Proceedings, 15-19 March 2026, San Diego, CA, USA,
The Minerals, Metals & Materials Series, pp. 555-566
DOI: 10.1007/978-3-032-13828-6_48

Modeling and Simulation Strategies of Micro-Casting from Titanium (Ti-6Al-4V) Swarf

[1]Arul Mozhi Varman J P*, [2]James Wainwright, [2]Wojciech Suder, [1]Tharmalingam Sivarupan, [1]
Konstantinos Georgarakis, [1]Konstantinos Salonitis, [1]Mark Jolly, [2]Stewart Williams

[1]Sustainable Manufacturing Systems Centre,
Faculty of Engineering and Applied Sciences, Cranfield University, United Kingdom

[2]Welding and Additive Manufacturing Centre,
Faculty of Engineering and Applied Sciences, Cranfield University, United Kingdom

*Corresponding Authors: a.jayaramanpalanivel@cranfield.ac.uk

Abstract

One way of reducing the CO_2 footprint for titanium alloys can be by the innovative re-use of machining by-products (swarf). This paper will present modeling and simulation for micro-sized casting in Ti-6Al-4V (Ti64) swarf, with the ultimate aim of the development of continuous casting applications. Finite Element (FE) modeling is employed to predict thermomechanical behaviour enabling optimisation of heat transfer coefficients for enhanced process control. Computational Fluid Dynamics (CFD) simulation is used to simulate melt flow within a micro-scale crucible to ensure reliable molten metal delivery. Using simulation tools enables rapid design iteration and process tuning without extensive trial-and-error experimentation. This work could contribute to circular economy practices and reinforces the role of digital twins in advancing net zero manufacturing goals in metal manufacturing processes.

Keywords: Titanium alloys, continuous casting, Finite Element Analysis, CFD Simulation, net zero

1. Introduction

Titanium alloys are extensively used in high-performance sectors such as aerospace and biomedical engineering. Over the past few decades, there has been a marked increase in their application, particularly in aviation, where titanium content per aircraft has grown significantly, reflecting the broader industry trend toward lightweight and high-strength materials [1]. Aerospace components, especially rotating parts, demand rigorous quality control due to their sensitivity to material impurities. Even trace levels of inclusions whether high-density (HDI) or low-density (LDI) can lead to premature failure [2]. To mitigate this, industry-standard practices include advanced remelting technologies designed to purify the metal. Hearth Melting (HM), conducted under vacuum or inert atmospheres, is one such technique. It offers extended dwell time in water-cooled copper crucibles, aiding in the dissolution of LDI and removal of HDI. The heat transfer coefficient of the crucible is optimised through numerical simulations and experimental validation[3]. The heat extraction depends on the cooling water flow and its velocity as validated by Ko et, al for the continuous casting of steel [4]. These practices have become standard in the titanium industry for more than 20 years, underpinning the reliability of critical aerospace and defense components[5].

However, a major challenge in titanium component manufacturing is the significant material loss during machining. Often, only half of the original billet or forged part is retained in the final product, with the rest lost as swarf or scrap. In extreme cases, up to 90% of the original material is wasted such as the case of Boeing 787 airframe production, where 100 tons of scrap can result from machining a 120-ton ingot [6] . Biomedical applications face similar inefficiencies; for example, machining of orthopaedic implants like knee joints results in up to 80% scrap [7].

Published by Springer. This is the Author Accepted Manuscript issued with: Creative Commons Attribution License (CC:BY 4.0).
The final published version (version of record) is available online at DOI:10.1007/978-3-032-13828-6_48. Please refer to any applicable publisher terms of use.

This inefficiency has prompted a push toward more sustainable practices and circular economy models within the titanium industry. Recent innovations in scrap recycling focus on transforming swarf and other titanium waste into usable material. In our earlier work, the concept of two-stage crucible method was used for melting and refining the titanium scraps. The model discusses the different components of heat losses such as radiation, conduction, and convection for a continuous/pulsed heat source. Also, the optimum bath surface temperature to capture the HDI inclusions while melting the LDI inclusions floating atop to obtaining a clean melt for continuous casting or other feedstock applications[8].

In this paper, the primary focus is to develop a micro sized continuous casting from the continuous feedstock of Ti64 swarfs/scraps. The major problems associated with melting of titanium alloys (Ti64) are (i) surface tension, and (ii) Marangoni convection which drives the molten liquid to flow [9], [10]. During wire arc additive manufacturing (WAAM) of Ti64 alloys the molten metal droplets are detached from the wire and deposited on the substrate. Different types of droplet transfer mechanisms are used to overcome the surface tension forces and thermal gradient to facilitate the detachment of the droplets from the wire [11]. However, at the microscale of casting, the problems look different as the main purpose is to hold the minimum liquid mass in the crucible for the reliable molten liquid delivery (outlet mass flow rate, m_{out}) through spout rather than continuously depositing the liquid in the case of WAAM.

Figure 1 shows the typical crucible (Material: Oxygen Free High Thermal Conductivity Copper) geometry used for both the experiments and simulation. This process is configured with the high energy laser sources for melting, thermocouples (T1 and T2) for temperature measurements. Cooling of the crucible is achieved by providing a heat sink with the high-pressure water circulation (W_{in} and W_{out}). The volume of liquid in the crucible is dependent on the inlet mass flow rate (m_{in}) which is defined as continuous material feeding in forms of either pellets or filler wires.

The major problem is to be quantifying the heat losses accurately. Heat losses are categorised as (i) radiation, (ii) convection, and (iii) conduction. These losses are captured and quantified using mathematical equations as presented in earlier work [8]. Optimizing the heat transfer coefficient of the crucible is crucial to prevent it from melting/over-heating. This can be achieved by numerical simulation using a range of heat transfer coefficients which provides a reasonable estimate. The following sections discuss the importance of liquid mass and the heat transfer coefficients.

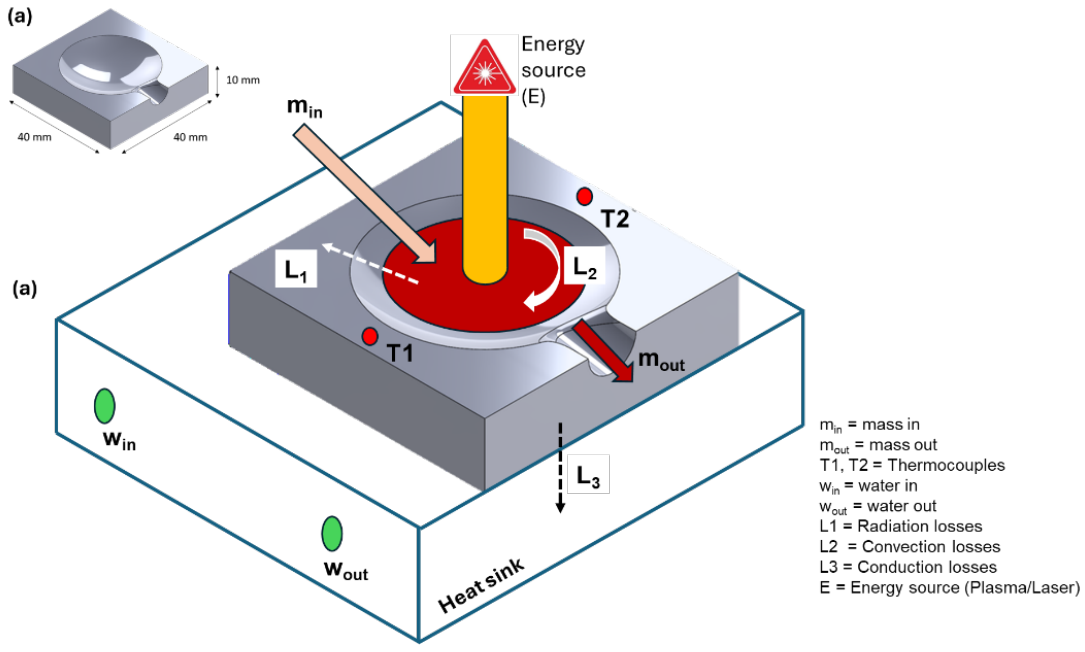

Figure 1 (a) CAD model of the crucible. All dimensions are in 'mm' (b) Schematic view of the crucible its configuration.

2. Simulation methodologies

A commercial CFD solver from FLOW-3D with the WELD module (2025R1) was used for solving the numerical equations of melting and liquid flow. The governing equations and the initial and boundary conditions are set based on our earlier work [8] . Additionally, the use of energy sources with associated physical properties are optimised based on WELD module library, user defined functions derived from various simulation iterations. A constant energy source using a laser with a power of 2 kW and a spot diameter of 6 mm was used based on the experimental conditions. Simple arc pressure with a gaussian distribution was applied along with the heat source [12]. A rectangular mesh with a 500 µm mesh size was used, and the total number of mesh cells was 1.3 million. A high-performance computing facility with the 32-core license solver running on a parallel computer was used for running 10 s physical simulation. But the actual wall time taken for the computational time is ~60 h.

Table 1 Thermophysical properties of TI6AI4V liquid

Parameters	Values
*Liquidus temperature, K	1923
*Solidus temperature, K	1873
Specific heat, J/Kg/K	546
Latent heat of fusion, kJ/kg	
Surface tension coefficient (kg/s^2)	1.33
*Viscosity, Kg/m/s	3.25 x 10^{-3}
emissivity	0.3
Thermal expansion coefficient, K^{-1}	9.0 x 10^{-6}
*Temperature dependent values are used	

To optimise the thermal distribution of the crucible, Finite Element Analysis (FEA) was performed using Ansys 2024 R2 Transient Thermal method for different heat convection coefficients (h_{conv}). Figure 2 shows the FE meshing and boundary conditions for the simulation. The assumptions considered for the simulation is that the liquid contact area inside the crucible is fixed with a temperature of 1933 K (10 K above the liquidus temperature) as shown in Figure 2(b) while h_{conv} is varied to study the crucible thermal distribution until steady state temperature is reached. The simulation was run for 300 s.

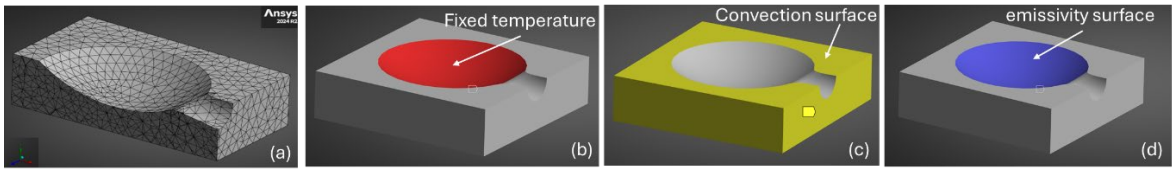

Figure 2 FE meshing and boundary conditions (a) Mechanical type with the element size of 5 x 10^{-4} m. Total nodes and elements are 24473 and 16494, respectively. Tet10 elements corresponds to 16493.

3. Results and discussions

3.1. Computational Fluid Dynamics (CFD) Analysis:

3.1.1. Influence of liquid mass on the outlet mass flow rate (m_{out})

The sensitivity analysis of the experiment shows that the mass flow rate is 0.28 g/s. The time for the liquid metal to build up in the crucible for delivering the first droplet is at 2.9 s. The second droplet delivery takes about 12.5 s. The time different between first and second droplet is around 9.6 s. Since, outlet mass flow rate (m_{out}) is dependent several factors such as mass flow rate of the inlet supply (m_{in}), energy needed for melting and heat transfer coefficient between the liquid and the crucible. However, the effect of surface tension forces and Marangoni convection can be overcome by optimising m_{in} and crucible tilt angle to avoid the thermal losses of the liquid which drives the molten metal flow as evidenced in the experiments. The relative viscosity of the liquid with respect to 2173 K (1900 °C) indicates that at the liquidus temperature of 1923 K (1650 °C), its viscosity is higher by 38% followed

by 28% and 13% at 1973 K (1700 °C) and 2073 K (1800 °C). So, molten liquid temperature plays a vital role in the liquid flow. The temperature of the liquid must be preserved until the crucible spout simultaneously increasing the liquid mass to drive the flow otherwise early solidification takes place at the spout retarding the liquid flow. This can be achieved by a combination of energy sources to provide adequate energy to the liquid.

Results from numerical simulations are compared with the experiments as shown in Figure 3 and Figure 4. Simulations with the low inlet mass flow rates of 0.28 g/s and 0.56 g/s, the liquid builds up until 10 s without flowing through the crucible spout. This indicates that the capturing all the physical aspects of the experiments in particular the liquid to crucible heat transfer coefficient is important for the simulation. As discussed earlier, the time interval between the first and second delivery of the metal is ~9.6 s whereas in the simulation there is no liquid delivery even for 0.56 g/s inlet mass flow rate. However, simulation with high inlet mass flow rate of 11.1 g/s the molten liquid flows out of the spout at 2.4 s during the 10 s simulation for a given liquid to crucible heat transfer coefficient of 1 $kW/m^2.K^{-1}$. Also, the maximum liquid temperature for the inlet mass flow rates of 0.56 g/s and 11.1 g/s reaches >3000 K and 2200 K, respectively. The actual measurement of the liquid temperature is around 2200 K which is closely matching with the simulation results for the case of 11.1 g/s inlet mass flow rate. The importance of heat transfer coefficient between the liquid and the crucible, and between the crucible and the ambient will be discussed shortly.

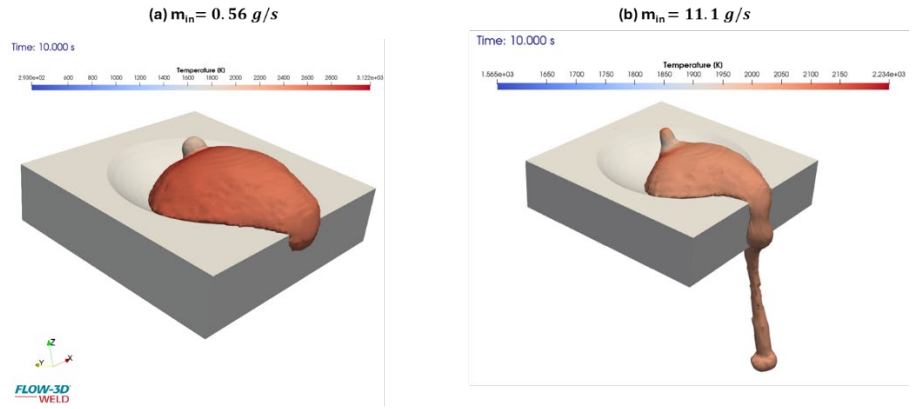

Figure 3 Influence of inlet mass flow rate (m_{in}) on the molten metal delivery through spout (m_{out}) (a) m_{in} =0.56 g/s, and (b) m_{in} =0.11 g/s.

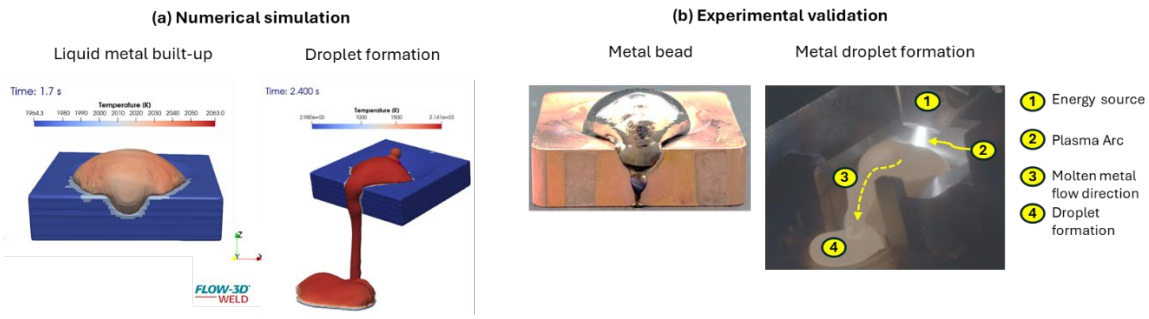

Figure 4 Comparison of molten metal liquid flow of (a) numerical simulation of 11.1 g/s inlet mass flow rate and (b) experimental validation of 0.28 g/s inlet mass flow rate.

Figure 4 (a) shows the simulation result with high inlet mass mas flow rate of 11.1 g/s where the amount of liquid piles up until 2.4 s before delivering the liquid through spout compared with experimental observation of 2.9 s for the low inlet mass flow rate of 0.28 g/s. To drive the molten liquid through spout the following aspects of components are crucial such as (i) thermal balance under dynamic conditions with respect to the liquid flow, (ii) constant inlet mass flow rate, (iii) multi-energy sources.

Additionally, in both cases, the profile of the liquid metal builds up looks similar until the delivery. Further characterisation on bead profile with the crucible will be done by slicing them together. This understanding is crucial to optimising the crucible's thermal distribution without causing melting or thermal damage. The melting phenomenon of the crucible can be avoided by providing additional energy source close to the spout and optimizing the geometrical parameter such as radius which connects crucible cavity and the delivery spout. In addition, the crucible positioning for example the tilt angle along the Y-direction which accelerates the flow due to the gravitational force and reduces the liquid residence time in the crucible. To achieve the desired flow rate (m_{out}) the liquid mass and the crucible tilt angle need to be optimised. Further experiments will be undertaken to validate the addition of (i) fixed energy source close to the spout or (ii) Scanning energy source along the spout. These experiments will focus on optimizing the liquid temperature for reliable delivery without early solidification in the crucible/spout.

The challenges experienced during experiments are (i) the inadequate flow of molten liquid metal which is a function m_{in} as shown in Figure 3, and (ii) the high interface temperature between the liquid (l) and the crucible (c) as shown in Figure 5. The interface temperature ($T_{l/c}$) is dependent on the crucible temperature which is controlled by the heat convection coefficient of the crucible. Usually, the crucible is water cooled using high pressure water to achieve the steady state temperature. The interface temperature ($T_{l/c}$) is dependent on (i) liquid temperature, (ii) liquid residence time, and (iii) heat transfer coefficient between liquid and crucible ($h_{l/c}$) which is dependent on the crucible heat transfer coefficient between the crucible and the ambient (high pressure water).

The interface between the liquid and the crucible is subjected to high thermal gradient. As a result, crucible temperature reaches close to its melting point and sometimes results in melting/burn-through as shown in Figure 5 for m_{in} of 11.1 g/s. Also, the melting of the crucible with m_{in} of 0.26 g/s compared to m_{in} of 11.1 g/s is higher due to the high melting temperature of the liquid with the longer liquid residence time in the crucible. The liquid residence time is crucial to prevent the crucible melting. It is necessary to optimise the liquid temperature to serve two purposes. The first one is to facilitate the liquid to flow down through spout smoothly, and the second is to prevent the melting of the crucible. Figure 5(a) shows thermal profile of the liquid contact area of the crucible and Figure 5(b) shows the sliced view with the focused view at the interface between the liquid/crucible. The crucible started to melt as the $T_{l/c}$ reached above the copper melting temperature and the depth of melting is calculated to be around 0.4 mm and the overall heat affected zone is around 0.8 mm. The melting of the crucible can be avoided by providing suitable heat transfer coefficients ($h_{l/c}$) as discussed in the next section.

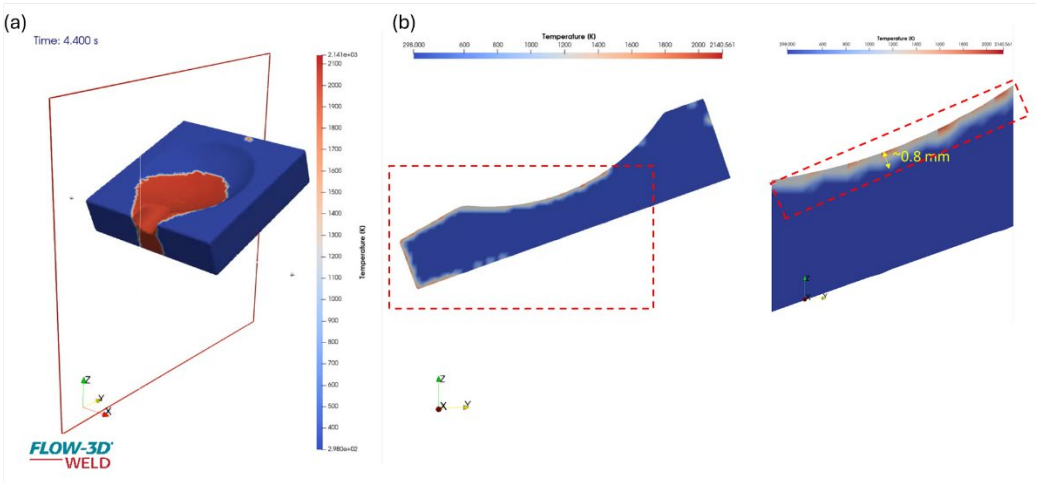

Figure 5 Thermal distribution of the crucible after 4.4 s for 11.1 g/s (a) Red region indicates the surface in contact with the hot liquid (b) Corresponding sliced view indicating the partial melting and heat affected zone.

3.2. Finite Element (FE) Analysis:

To overcome the high temperature and/or burn through of the crucible it is essential to provide adequate cooling mechanisms to balance the thermal energy of the melting and continuous casting process. This challenging task is undertaken by capturing all the possible losses as close to the real experiments. Since the copper crucible begins to deform around 1173 K, the operating temperature of the crucible needs to be well below to it. Figure 6 shows the FE simulation results for different heat convection coefficients. As the heat convection coefficients (h_{conv} is defined as the heat transfer coefficient between the crucible surfaces and the ambient atmosphere at 298 K (25 °C) increases the average temperature of the crucible decreases and the heat flow to the surround increases. To operate the crucible well below its melting temperature a typical h_{conv} of 30 kW/m^2.K^{-1} is required which is a reasonable value for such applications. The corresponding heat flow is around 85 kW for the present crucible surface area considerations.

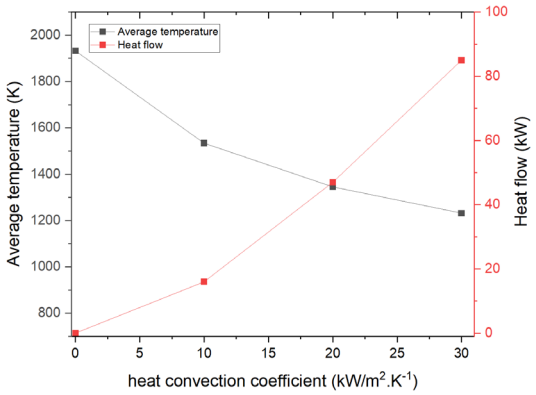

Figure 6 Influence of different heat convection coefficient (for different cooling types) on thermal distribution of the crucible.

Sectional view of FE simulation results for different h_{conv} is shown in Figure 7. The red region is in contact with the liquid which is assumed to be at 1933 K (1660 C) which is 10 K above the liquidous temperature of 1923 K (1650 C). The thermal profile indicates the different zone with varied temperatures.

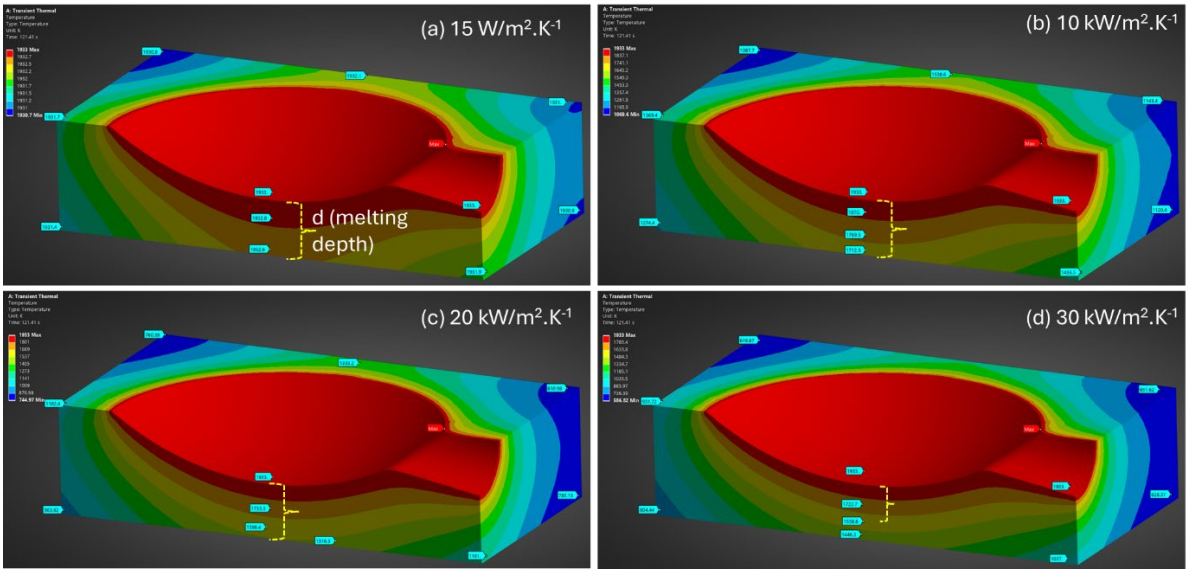

Figure 7 FE simulated thermal profile of the crucible for different heat convection coefficients (a) 15 W/m^2.K^{-1} (b) 10 kW/m^2.K^{-1}(c)20 kW/m^2.K^{-1}(d) 30 kW/m^2.K^{-1}

FE simulations with ambient heat transfer convection coefficient (15 $W/m^2.K^{-1}$) indicates complete melting of the crucible as denoted by d (melting depth). The temperature of the crucible at the top surface which is in contact with the liquid, and the bottom surface which is in contact with the heat sink indicates how steep is thermal gradient for different h_{conv}. A higher h_{conv} means lower melting depth, higher heat flow with lower crucible temperature. In addition, thermal profile indicates thermal concentrated region where the possibility to further optimising the crucible design is identified and iterated until thermal profiles are within the acceptable range.

The limitations of the present simulation case are (i) No interface heat transfer coefficient is applied between the liquid to the crucible, and (ii) No physical skull formation between the liquid and the crucible. Further to improve the model the interfacial heat transfer coefficients and a methodology to incorporate the skull zone will be modeled using Griffith's work [13], [14] followed by temperature measurements at appropriate locations of the crucible for validation and to refining the numerical parameters for the simulations.

4. Conclusions

An attempt to model the melting and continuously casting the Ti64 alloy in lower quantities showed promising results. CFD simulated inlet mass flow rate is closely matching with the experimented mass flow rate. Low inlet mass flow rate (m_{in}= 0.28 g/s) resulted in early solidification close to the spout with the high liquid temperature (3000 K) beneath the laser spot at the liquid surface. However, to achieve the continuous droplets without melting/overheating of the crucible, the minimum mass required is 11.1 g/s compared to 0.28 g/s of the experiment. This resulted in good Marangoni convection and reduced the surface tension gradient.

Further studies to optimising the interface heat transfer coefficients between different components such as liquid, skull, crucible and the ambient will be explicitly studied using iterative simulations. FE Simulation results showed that for $h_{conv} \geq 30$ $W/m^2.K^{-1}$, the crucible thermal distribution is well below its melting temperature while the scope to modify the crucible design is identified for future studies.

Acknowledgments

The project was funded by an EPSRC Programme Grant SAM (EP/W01906X/1). We would like to acknowledge the supports from Cranfield University (HPC resources) and Flow Science, US.

References

[1] V. Tebaldo, G. Gautier di Confiengo, D. Duraccio, and M. G. Faga, "Sustainable Recovery of Titanium Alloy: From Waste to Feedstock for Additive Manufacturing," Jan. 01, 2024, *Multidisciplinary Digital Publishing Institute (MDPI)*. doi: 10.3390/su16010330.

[2] H. Holst, "Study of the Influence of the Plasma Torch in a Plasma Arc Melting Furnace," 2015.

[3] J. P. Bellot *et al.*, "Numerical Simulation of the Plasma Arc Melting Cold Hearth Refining Process (PAMCHR)," *Metallurgical and Materials Transactions B: Process Metallurgy and Materials Processing Science*, vol. 51, no. 4, pp. 1329–1338, Aug. 2020, doi: 10.1007/s11663-020-01866-0.

[4] E. Y. Ko, K. W. Yi, J. K. Park, J. W. Cho, and H. J. Shin, "Numerical modeling and analysis of the thermal behavior of copper molds in continuous casting," *Metals and Materials International*, vol. 16, no. 2, pp. 281–288, 2010, doi: 10.1007/s12540-010-0418-8.

[5] M. J. , Blackburn and D. R. , Malley, "Plasma arc melting of titanium alloys," *Mater Des*, vol. 14, no. 1, pp. 19–27, 1993.

[6] O. Takeda and T. H. Okabe, "Current Status of Titanium Recycling and Related Technologies," Jun. 15, 2019, *Minerals, Metals and Materials Society*. doi: 10.1007/s11837-018-3278-1.

[7] L. E. Murr *et al.*, “Microstructure and mechanical behavior of Ti-6Al-4V produced by rapid-layer manufacturing, for biomedical applications,” Jan. 2009. doi: 10.1016/j.jmbbm.2008.05.004.

[8] J. P. A. M. Varman, T. Sivarupan, K. Georgarakis, K. Salonitis, and M. Jolly, “Modeling and Simulation of Cold Hearth Continuous Casting of Titanium Alloys,” in *Minerals, Metals and Materials Series*, Springer Science and Business Media Deutschland GmbH, 2025, pp. 1117–1124. doi: 10.1007/978-3-031-80676-6_139.

[9] W. Suder *et al.*, “Control of meltpool shape in laser welding,” *Welding in the World*, vol. 68, no. 6, pp. 1485–1495, Jun. 2024, doi: 10.1007/s40194-024-01719-3.

[10] X. Zhou, H. Zhang, G. Wang, and X. Bai, “Three-dimensional numerical simulation of arc and metal transport in arc welding based additive manufacturing,” *Int J Heat Mass Transf*, vol. 103, pp. 521–537, Dec. 2016, doi: 10.1016/j.ijheatmasstransfer.2016.06.084.

[11] S. Ríos, P. A. Colegrove, and S. W. Williams, “Metal transfer modes in plasma Wire + Arc additive manufacture,” *J Mater Process Technol*, vol. 264, pp. 45–54, Feb. 2019, doi: 10.1016/j.jmatprotec.2018.08.043.

[12] X. Chen, C. Wang, J. Ding, P. Bridgeman, and S. Williams, “A three-dimensional wire-feeding model for heat and metal transfer, fluid flow, and bead shape in wire plasma arc additive manufacturing,” *J Manuf Process*, vol. 83, pp. 300–312, Nov. 2022, doi: 10.1016/j.jmapro.2022.09.012.

[13] C. P. Hallam and W. D. Griffiths, “A Model of the Interfacial Heat-Transfer Coefficient for the Aluminum Gravity Die-Casting Process.”

[14] W. D. Griffiths, “A Model of the Interfacial Heat-Transfer Coefficient during Unidirectional Solidification of an Aluminum Alloy.”

https://dspace.org/

Modeling and simulation strategies of micro-casting from titanium (Ti-6Al-4V) swarf

Mozhi Varman, J. P. Arul; Wainwright, James; Suder, Wojciech; Sivarupan, Tharmalingam; Georgarakis, Konstantinos ...

2026-03-02
Springer
https://doi.org/10.1007/978-3-032-13828-6_48
Mozhi Varman JPA, Wainwright J, Suder W, et al., (2026) Modeling and simulation strategies of micro-casting from titanium (Ti-6Al-4V) swarf. In: TMS 2026 155th Annual Meeting & Exhibition Supplemental Proceedings, 15-19 March 2026, San Diego, CA, USA, The Minerals, Metals & Materials Series, pp. 555-566

Downloaded from a DSpace repository. https://dspace.org/